

# Cleavage Fracture in Continuously Cooled V-Microalloyed Medium Carbon Steel

D. Glišić, N. Radović, D.J. Drobñjak and A. Fadel

**Abstract** Medium carbon V-microalloyed steel continuously cooled from the austenitization temperature at still air, with predominantly acicular ferrite structure, has been investigated by means of four-point bending of notched Griffiths–Owens’s type specimens at liquid nitrogen temperature. Local fracture stress and plastic strain were determined by using finite element analysis and fracture surface examination using scanning electron microscope. It was revealed that cleavage fracture initiation, which takes place close to the notch root in the narrow zone of high plastic strains, is not related to any broken coarse second phase particles. It was assumed that microcracks nucleate by strain induced fracture of pearlite nodules. Two effective surface energy values of 24 and 42 J/m<sup>2</sup> were estimated according to the Griffith’s equation, indicating the influence of crystallographic orientation between neighboring grains at the origin of fracture. Lower value was attributed to fracture of coarse ferrite–pearlite units with similar crystallographic orientation and higher value to fracture propagation through fine acicular ferrite matrix.

**Keywords** Micro-alloyed steel · Cleavage stress · Surface energy

## 1 Introduction

Microalloyed medium carbon forging steels are designed in attempt to attain required strength of forged parts by direct cooling from the hot working temperature, thus eliminating expensive procedure of quenching and tempering. Microalloying elements increase strength of the steels through grain refinement and

---

D. Glišić (✉) · N. Radović · D.J. Drobñjak  
Faculty of Technology and Metallurgy, University of Belgrade, Karnegijeva 4,  
11120 Belgrade, Serbia  
e-mail: gile@tmf.bg.ac.rs

A. Fadel  
Al Zawiya University, Zawiya, Libya

precipitation of fine carbo-nitride particles. Although satisfactory strength level and fatigue properties are achieved, toughness of the continuously cooled microalloyed forging steels is much lower compared to that of quenched and tempered steels. An improvement of the toughness is observed in microalloyed steels with acicular ferrite present as dominant in the structure [20, 22]. It is believed that fine randomly oriented interlocking ferrite plates and laths provide additional barriers for cleavage crack propagation [22, 24].

Cleavage fracture of continuously cooled medium carbon microalloyed steels has been studied prevalently for ferrite–pearlite and bainite structures, while the steels with predominantly acicular ferrite structure received relatively limited attention [11, 16].

The aim of present work is to assess cleavage fracture mechanism in continuously cooled medium carbon V-microalloyed steel with predominantly acicular ferrite structure.

## 2 Material and Experiment

Samples of commercial V-microalloyed medium carbon hot-rolled steel rods 19 mm in diameter, with chemical composition given in Table 1, have been heat-treated with intention to obtain acicular ferrite in the structure by cooling at still air directly from the austenitization temperature. In order to eliminate as-received microstructure specimens were initially homogenized at 1250 °C for 4 h in argon protective atmosphere followed by oil quenching. Specimens were then austenitized at 1250 °C for 30 min in argon atmosphere and cooled at still air.

The cleavage fracture strength was measured via four-point bending (4 PB) testing at constant crosshead speed of 0.1 mm/min in liquid nitrogen (−196 °C) using Griffiths–Owens’s specimen (12.7 × 12.7 × 75 mm with 45° notch 4.23 mm deep and with radius of 0.250 mm) [18].

Fracture surface was analyzed by scanning electron microscope (SEM) equipped with energy dispersive X-ray spectrometer (EDS). The cleavage initiation sites were identified by tracing chevron stripes at lower magnifications and river pattern lines at higher magnifications back to the cleavage origin. Cleavage origin distance from the notch root and cleavage facets sizes were measured from the SEM micrographs.

Stresses and strains ahead of the notch root of the four-point bending specimen were calculated by finite element analysis (FEA) using ABAQUS code. The specimen was modeled in two dimensions with quadratic eight-node plane strain elements (CPEG8). Material’s elastic properties were represented by Young’s modulus of 200 GPa, Poisson’s ratio of 0.28 [18]. Plastic response was modeled by experimentally determined true stress–strain curve. True stress–strain curve were obtained by polynomial regression of experimental data obtained by uniaxial tensile test at liquid nitrogen temperature. Tensile testing was performed at constant crosshead speed of 0.1 mm/min, which corresponds to that of four-point bending. Specimens 6 mm in diameter and with 30 mm gauge length were used [17].

**Table 1** Chemical composition of the tested steel (in wt.%)

C	Si	Mn	P	S	Cr	Ni	Mo	V	Ti	Al	Nb	N
0.256	0.416	1.451	0.0113	0.0112	0.201	0.149	0.023	0.099	0.002	0.038	0.002	0.0229

### 3 Results and Discussion

Typical microstructure of the steel is shown in Fig. 1. Grain boundary ferrite idiomorphs (GBF) form continuous network along previous austenite grain boundaries. Some allotriomorphs could be observed, sometimes with Widmanstätten saw-teeth (WST) ferrite plates that have nucleated on them (Fig. 1a). Most of the grain interiors are occupied by acicular ferrite (AF) typically bordered by pearlite nodules (P) and grain boundary idiomorphs (GBI) (Fig. 1b).

During cooling from austenitization temperature, proeutectoid ferrite is formed along austenite grain boundaries. Due to low solubility in ferrite, carbon diffuses into neighboring austenite. This local enrichment on carbon increases the stability of present austenite until  $A_{r1}$  temperature is reached when diffusional transformation to pearlite occurred. At lower temperatures, when diffusion becomes sluggish, remained austenite transforms by bainitic mechanism. Since grain boundaries are already occupied by ferrite grains, grain boundary nucleation of bainitic sheaves is precluded, and therefore intragranular nucleation of acicular ferrite takes place. Intragranular nucleation of acicular ferrite is promoted by second phase particles, which act as a ferrite nucleation sites. Among them, most potent for acicular ferrite nucleation are vanadium-carbonitride particles [14, 20], which could be expected in the present case, considering chemical composition of the steel.

Fracture surfaces of all tested four-point bending samples, shown in Fig. 2a–d, exhibit typical transgranular brittle fracture. Fracture surface is characterized by mixture of small irregular cleavage facets that surround coarse, usually elongated facets. Chevron lines clearly point to the zone of cleavage initiation, which is for all specimens placed near the notch root. Fine river lines are clearly visible on coarse facets, but on small facets seem to be finer and somewhat difficult to trace toward the cleavage origin.

Moreover, twisted or greatly tilted cleavage planes of small facets indicate high crystallographic misorientation. Such frequent change of crack propagation

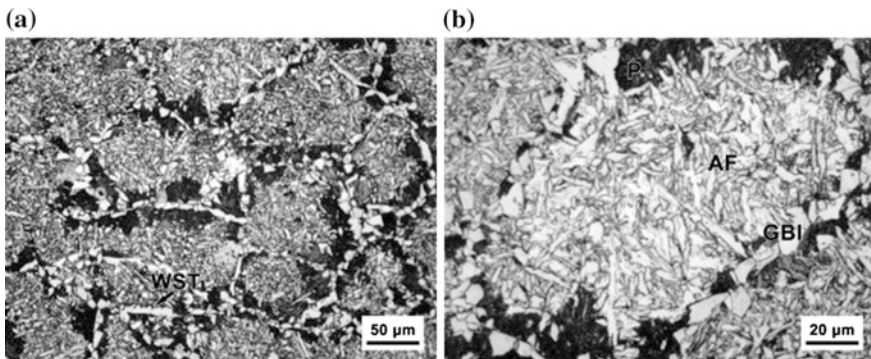


**Fig. 1** Microstructure of the tested steel; *WST* Widmanstätten saw-teeth ferrite, *P* pearlite, *GBI* grain boundary idiomorphs, *AF* acicular ferrite

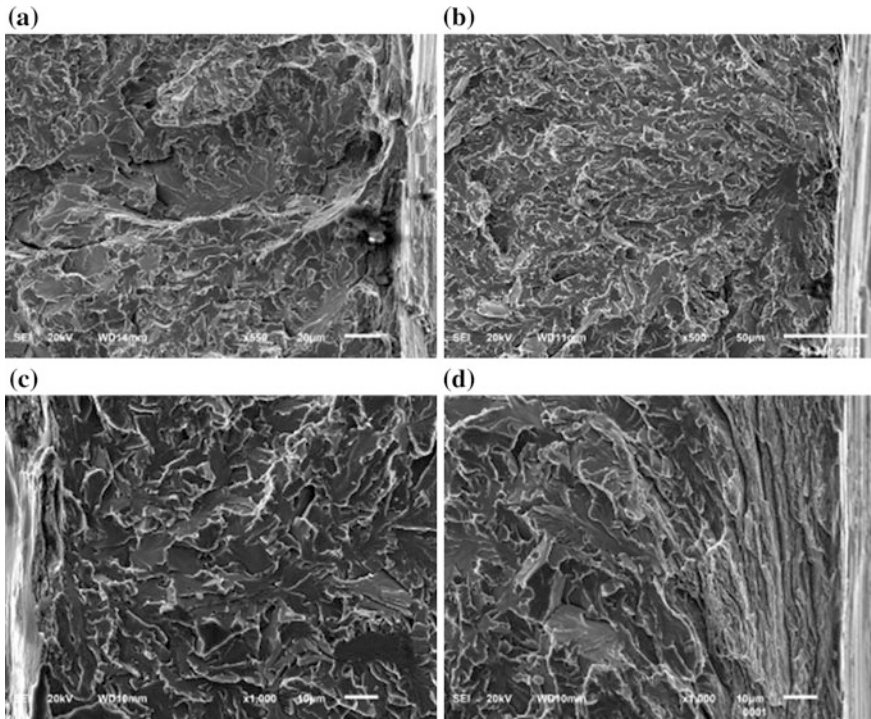


**Fig. 2** Fracture surfaces near the fracture initiation site

direction and elevation clearly reflects underlying fine interlocked structure of acicular ferrite. Consequently, many local crack branches and deep side microcracks could be observed.

Small facets connected by uninterrupted surface traces, tilted at low angles, could be ascribed to cleaved sheaves of acicular ferrite laths or plates with low crystallographic misorientation. It had been established that acicular ferrite formed at lower temperature range, around 400–450 °C, consists of sheaves of nearly parallel laths and plates with similar crystallographic orientation [8, 19]. Acicular ferrite formed in higher temperature range is characterized by higher density of fine ferrite laths or plates with high crystallographic misorientation [8, 12, 19]. It is assumed that continuously cooled acicular ferrite would consist of mixture of both types. Although some of the coarse laths observable in micrograph in Fig. 1b could be recognized as a sheaf of nearly parallel acicular ferrite laths/plates, it is not actually possible to distinguish different types of acicular ferrite at light microscopy level. As it had been established, only high angle boundaries, with misorientation angle higher than 15°, could be an effective barrier to cleavage crack propagation and morphological size does not correspond to “effective” or crystallographic packet size [8, 26].

Coarse elongated facets correspond to some large microconstituent or a group of grains with similar crystallographic orientation. In medium carbon steels such large grains belong to ferrite–pearlite aggregates with the same crystallographic orientation, which is easily trespassed by propagating crack [25].

As could be observed from the SEM micrographs in Fig. 2a–d, cleavage origin is located almost at the notch root. Distances of the initiation site from the notch root,  $X_0$ , summarized in Table 2 among other measured values, range from only 14 to 56  $\mu\text{m}$ . Second phase particles have not been found at the origin. Similar case of the cleavage initiation at the notch root of a microalloyed medium carbon steel with acicular ferrite structure had been reported earlier [9]. Cleavage fracture of medium carbon microalloyed steels with ferritic–pearlitic, bainitic or martensitic structure is usually related to the fracture of coarse second phase particles. In most cases of the microalloyed steels, broken TiN or complex (Ti,V)(C,N) particles were responsible for cleavage initiation, but also fractured or delaminated MnS inclusion, other complex particles or fractured coarse carbides in the zone of high stress intensification [2–4, 13, 27].

Stress and strain distribution along the distance from the notch root, calculated by FEM analysis, is shown in Fig. 3. Cleavage initiation is located in the narrow zone of high plastic strains (shaded area in the graph), where maximum principal stress is relatively low. The values of the principal plastic strain at the location of cleavage origin,  $\epsilon_{pc}$ , range from 0.19 to 0.35, while local fracture stress,  $\sigma_F^*$ , does not exceed 1672 MPa. Considering that stresses for fracture of particles in microalloyed medium carbon steels with various microstructures is approximately 2500 MPa [10, 23], it is clear that cleavage initiation by this mechanism could not be expected near the notch root. Fracture of coarse particles should be expected around 400–600  $\mu\text{m}$  away from the notch, where peak values of principal stress,  $\sigma_{1max}$ , reach between 2360 and 2589 MPa (Fig. 3 and Table 1).

Plastic strains in this zone are considerably lower implying that critical flaw had been formed under the influence of high plastic strains near notch root. Critical value of plastic strain had been proposed earlier by Chen et al. [5, 6]. They

**Table 2** Values measured in the four-point bending test at  $-196\text{ }^\circ\text{C}$  and calculated values of local fracture stress and plastic strain at the origin of fracture

$F_{max}$ (N)	$\sigma_F$ (MPa)	$\sigma_F/\sigma_Y$ (MPa)	$\sigma_{1max}$ (MPa)	$X_0$ ( $\mu\text{m}$ )	$\sigma_F^*$ (MPa)	$\epsilon_{pc}$	$D_{max} \times D_{min}$ ( $\mu\text{m}$ )	$D_{eff}$ ( $\mu\text{m}$ )	$\gamma$
28,521.6	1192.7	1.54	2524.7	32	1556.1	0.26	$36.8 \times 15.5$	24.5	87.0
				53	1671.5	0.22	$12.8 \times 17.3$	11.9	48.7
30,318.1	1267.8	1.64	2588.6	19	1484.3	0.35	$23.7 \times 9.8$	15.6	50.3
				19	1484.3	0.35	$21.0 \times 11.3$	16.7	53.9
				28	1545.1	0.33	$29.3 \times 24.1$	28.5	99.9
25,084.6	1049.0	1.35	2360.0	15	1433.2	0.20	$41.0 \times 8.1$	14.0	42.1
				14	1430.5	0.20	$8.6 \times 6.8$	8.3	24.8
27,561.2	1152.5	1.49	2474.2	56	1669.4	0.19	$34.7 \times 8.2$	14.0	57.4
				54	1662.4	0.19	$10.7 \times 3.7$	6.0	24.4

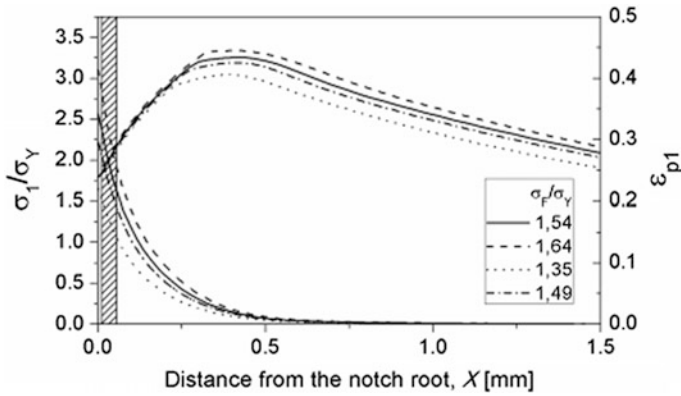
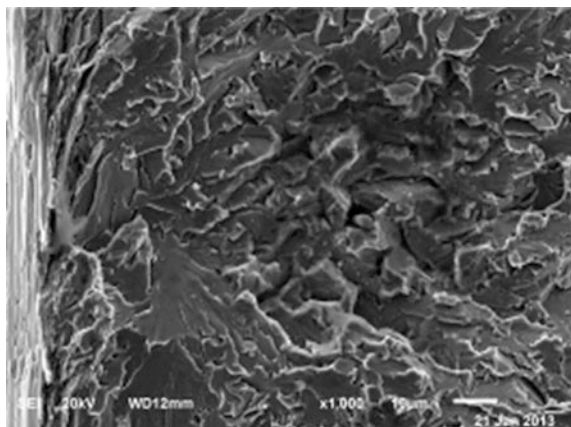


**Fig. 3** Distribution of the maximum principal stress and plastic strain along the distance from the notch root for all samples

suggested that critical strain must be attained for microcrack nucleation, critical stress triaxiality to prevent crack from blunting at stress level to provide further crack propagation [6]. Nevertheless, it remains unclear why particles remain inactive in a presence of acicular ferrite structure. Aside the fact that present steel contains negligible amount of titanium added, other aforementioned coarse particles or inclusions could be the candidate for cleavage nucleation. An example of broken particle at the fracture surface, which is not the origin of the fracture, is shown in Fig. 4. Elongated cylindrical form of the particle is typical for the MnS modified by calcium addition. It is apparently surrounded by a cluster of small facets, likely related to the acicular ferrite plates/laths, while the main crack path emanating from the coarse facets at the cleavage origin traverse them. Large facet probably belongs to ferrite–pearlite grains with same crystallographic orientation that was easily surpassed by advancing cleavage crack.

**Fig. 4** An example of broken inclusion (in the *middle*), not related to the fracture initiation site (to the *left*)



Two mechanisms of strain induced critical microcrack formation should be taken into account. According to the model proposed by Smith, grain boundary carbide fractures under the influence of stress field ahead of the dislocation pile-ups [28]. However, it had been established that Smith's mechanism is not applicable in the case of fine pearlite [21]. Based on the investigations of cleavage fracture in fully pearlitic steels, authors proposed that critical flaw is created by accumulation of damage within the pearlite colonies under the influence of plastic strain. Having in mind the presence of grain boundary ferrite and neighboring pearlite with similar crystallographic orientation in the microstructure of the steel investigated (Fig. 1) it seems that the latter mechanism is more applicable. Strain induced fracture of coarse ferrite–pearlite unit could create a critical flaw that would propagate further through the matrix at relatively low stress. As it was established, microcracks formed within ferrite or pearlite propagates through low angle boundaries of ferrite–pearlite units with same crystallographic orientation uninterruptedly [15, 25].

Since there were no particles at the cleavage origin, it was difficult to distinguish first cleavage facet. Therefore, two or three facets were measured, assuming they correspond to the initial microcrack. Maximum and minimum ferret diameters of the first facets measured are presented in Table 2, alongside with the effective crack diameter,  $D_{\text{eff}}$ , calculated using following equation [1, 9]:

$$D_{\text{eff}} = \frac{D_{\text{min}} \pi^2}{\phi^2 \cdot 4} \quad (1)$$

$$\phi = \frac{3\pi}{8} + \frac{\pi}{8} \left( \frac{D_{\text{min}}}{D_{\text{max}}} \right) \quad (2)$$

By considering determined values of local fracture stress,  $\sigma_F^*$ , and values of effective diameter of the first cleavage facet,  $D_{\text{eff}}$ , effective surface energy,  $\gamma$ , can be calculated from Griffith's equation for penny-shaped microcrack [7, 9]:

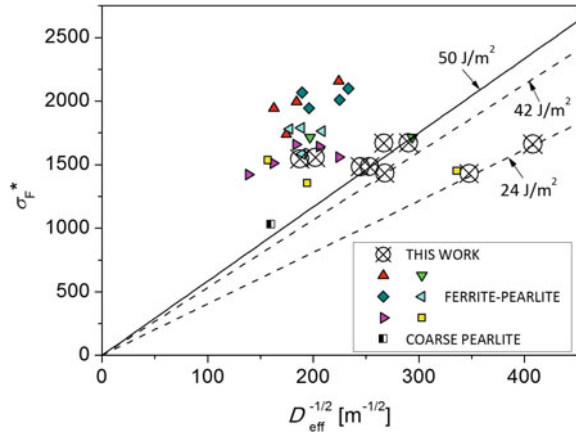
$$\sigma_F^* = \sqrt{\frac{\pi \cdot E \cdot \gamma}{(1 - \nu^2) \cdot D_{\text{eff}}}} \quad (3)$$

Calculated values of the effective surface energy,  $\gamma$ , are listed in Table 1, along with corresponding local fracture stresses and first facet diameters. The values of effective surface energy are in the range of 24–100 J/m<sup>2</sup>.

Local fracture stress is plotted against reciprocal value of square root of the effective diameter in Fig. 5. The lower bounds of the effective surface energies represented by the straight lines below two groups of points that correspond to coarse and fine facets, may be considered as an upper limit value, because it is higher or equal to the “real” value for given microstructure of the steel examined.



**Fig. 5** Values of the local critical fracture stress plotted against first cleavage facet's effective diameter and comparison with the values from literature [25, 27]



Method used here had been adopted from the Linaza, Echeverria and coworkers, who have calculated values of approx. 50 J/m<sup>2</sup> for ferrite–pearlite microalloyed medium carbon steels [25, 27]. Values from this work are plotted in Fig. 5 for the purpose of comparison. The first group of points from this work is somewhat lower. Unusually low values of the second group of points in present work are higher than values reported for fracture initiation on broken TiN particles, approx. 7 J/m<sup>2</sup> [25]. Cleavage initiation by fracture of the coarse second phase particles in present case could be considered as competing mechanism that has not been operative, or has been precluded by other process of initial microcrack nucleation. Therefore, it could be concluded that observed facets with small diameters, corresponding to lower values of effective surface energy, are related to fractured pearlite nodules. These pearlite nodules are between proeutectoid ferrite grains, along previous austenite grain boundaries, and acicular ferrite in the previous austenite grain interiors.

Relatively large initial microcracks formed in the zone of high plastic deformation near the notch root, require comparatively small stresses to propagate, in accordance to Griffith’s equation. Initial microcrack easily propagates through the matrix regardless of its size. However, two values of effective fracture energies from the graph in Fig. 5, of 24 and 42 J/m<sup>2</sup>, imply the effect of the underlying microstructure on initial microcrack propagation. The values of effective surface energy calculated here are comparable to the values determined in previous investigations found in literature for microalloyed medium carbon steels [25, 27]. It could be assumed that large initial microcrack is necessary to propagate through the matrix consisting of fine acicular ferrite laths/plates. Conversely, initial microcrack easily propagates when it encounters another pearlite nodule or ferrite grain with small crystallographic misorientation, rendering lower bound values of effective surface energy.

## 4 Conclusion

1. Cleavage fracture of the prevalently acicular ferrite steel, with ferrite and pearlite along previous austenite grain boundaries, was initiated by strain induced fracture of pearlite nodules and uninterrupted propagation through bordering ferrite grain or pearlite nodule with similar crystallographic orientation.
2. Effective surface energies of 24 and 42 J/m<sup>2</sup> were calculated using Griffith's–Owen approach. The latter value is in agreement with previously reported, although somewhat lower. Dual values of the effective surface energy were ascribed to differences in continuously cooled microstructure.
3. Although strain induced microcracks propagate at low stresses near the notch, local fracture stress and effective surface energy depend on propagation stage of the cleavage process and is affected by the microstructure surrounding initial microcrack. Propagation of the small facets, approximately 6–8 μm in diameter, is related to propagation through the matrix with small crystallographic misorientation. Inversely, larger initial microcracks are surrounded by finer grains that are related to the acicular ferrite structure.

## References

1. Alexander DJ, Bernstein IM (1989) Cleavage fracture in pearlitic eutectoid steel. *Metall Trans A* 20:2321–2335
2. Balart MJ, Davis CL, Strangwood M (2004) Observations of cleavage initiation at (Ti, V)(C, N) particles of heterogeneous composition in microalloyed steels. *Scr Mater* 50:371–375
3. Balart MJ, Davis CL, Strangwood M (2000) Cleavage initiation in Ti–V–N and V–N microalloyed ferritic–pearlitic forging steels. *Mater Sci Eng A* 284:1–13
4. Balart MJ, Davis CL, Strangwood M, Knott JF (2005) Cleavage initiation in Ti–V–N and V–N microalloyed forging steels. *Mater Sci Forum* 500:729–736
5. Chen JH, Wang GZ, Wang Q (2002) Change of critical events of cleavage fracture with variation of microscopic features of low-alloy steels. *Metall Mater Trans* 33A:3393–3402
6. Chen JH, Wang Q, Wang GZ, Li Z (2003) Fracture behavior at crack tip—a new framework for cleavage mechanism of steel. *Acta Mater* 51:1841–1855
7. Curry DA, Knott JF (1978) Effect of microstructure on cleavage fracture stress in steel. *Metal Sci* 12:511–514
8. Díaz-Fuentes M, Iza-Mendia A, Gutiérrez I (2003) Analysis of different acicular ferrite microstructures in low-carbon steels by electron backscattered diffraction. Study of their toughness behavior. *Metall Mater Trans A* 34:2505–2516
9. Echeverria A, Rodriguez-Ibabe JM (2003) The role of grain size in brittle particle induced fracture of steels. *Mater Sci Eng A* A346:149–158
10. Echeverria A, Rodriguez-Ibabe JM (2004) Cleavage micromechanisms on microalloyed steels. Evolution with temperature of some critical parameters. *Scr Mater* 50:307–312
11. Fadel A, Glišić D, Radović N, Drobnjak DJ (2012) Influence of Cr, Mn and Mo addition on structure and properties of V microalloyed medium carbon steels. *J Mater Sci Technol* 28:1053–1058
12. Fadel A, Glišić D, Radović N, Drobnjak DJ (2013) Intragranular ferrite morphologies in medium carbon vanadium-microalloyed steel. *J Min Metall Sect B Metall* 49:237–244

13. Fairchild DP, Howden DG, Clark WAT (2000) The mechanism of brittle fracture in a microalloyed steel, part I: inclusion-induced cleavage. *Mater Sci Eng A* 31A:641–652
14. García-Mateo C, Capdevila C, Caballero FG, De Andrés CG (2008) Influence of V precipitates on acicular ferrite transformation part 1: the role of nitrogen. *ISIJ Int* 48:1270–1275
15. Ghosh A, Ray A, Chakrabarti D, Davis CL (2013) Cleavage initiation in steel: competition between large grains and large particles. *Mater Sci Eng A* 561:126–135
16. Glišić D, Radović N, Koprivica A, Fadel A, Drobnjak DJ (2010) Influence of reheating temperature and vanadium content on transformation behavior and mechanical properties of medium carbon forging steels. *ISIJ Int* 50:601–606
17. Glišić D, Fadel A, Radović N, Drobnjak DJ, Zrilić M (2013) Deformation behavior of two continuously cooled vanadium microalloyed steels at liquid nitrogen temperature. *Hem Ind* 67:981–988
18. Griffiths JR, Owen DR (1971) An elastic–plastic stress analysis for a notched bar in plane strain bending. *J Mech Phys Solids* 19:419–431
19. Gutiérrez I, Díaz-Fuentes M (2003) Analysis of different acicular ferrite microstructures generated in a medium-carbon molybdenum steel. *Mater Sci Eng A* 363:316–324
20. Ishikawa F, Takahashi T (1995) The formation of intragranular ferrite plates in medium-carbon steels for hot-forging and its effect on the toughness. *ISIJ Int* 35:28–33
21. Lewandowski JJ, Thompson AW (1987) Micromechanisms of cleavage fracture in fully pearlitic microstructures. *Acta Metall* 35:1453–1462
22. Linaza MA, Romero JL, Rodríguez-Ibabe JM, Urcola JJ (1993) Improvement of fracture toughness of forging steels microalloyed with titanium by accelerated cooling after hot working. *Scr Metall Mater* 29:1217–1222
23. Linaza MA, Romero JL, Rodríguez-Ibabe JM, Urcola JJ (1995) Cleavage fracture of microalloyed forging steels. *Scr Metall Mater* 32:395–400
24. Linaza MA, Romero JL, San Martín I, Rodríguez-Ibabe JM, Urcola JJ (1996) Improvement of toughness by stopping brittle process nucleated in ceramic particles through thermomechanically optimized microstructures in engineering steels. In: Van Tyne CJ, Krauss G, Matlock DK (eds) *Microalloyed bar and forging steels*. TMS, Golden, p 311
25. Linaza MA, Rodríguez-Ibabe JM, Urcola JJ (1997) Determination of the energetic parameters controlling cleavage fracture initiation in steels. *Fatigue Fract Eng Mater Struct* 20:619–632
26. Rancel L, Gómez M, Medina SF, Gutierrez I (2011) Measurement of bainite packet size and its influence on cleavage fracture in a medium carbon bainitic steel. *Mater Sci Eng A* 530:21–27
27. Rodríguez-Ibabe JM (1998) The role of microstructure in toughness behaviour of microalloyed steels. *Mater Sci Forum* 284–286:51–62
28. Smith E (1968) Cleavage fracture in mild steel. *Int J Fract Mech* 4:131–145